846–860 *Nucleic Acids Research, 2017, Vol. 45, No. 2* *Published online 28 November 2016*
doi: 10.1093/nar/gkw1152

The Rrp6 C-terminal domain binds RNA and activates the nuclear RNA exosome

Elizabeth V. Wasmuth[1] and Christopher D. Lima[1,2,*]

[1]Structural Biology Program, Sloan Kettering Institute, Memorial Sloan Kettering Cancer Center, 1275 York Avenue, New York, NY 10065, USA and [2]Howard Hughes Medical Institute, Sloan Kettering Institute, Memorial Sloan Kettering Cancer Center, 1275 York Avenue, New York, NY 10065, USA

Received May 19, 2016; Revised October 17, 2016; Editorial Decision November 02, 2016; Accepted November 03, 2016

ABSTRACT

The eukaryotic RNA exosome is an essential, multi-subunit complex that catalyzes RNA turnover, maturation, and quality control processes. Its non-catalytic donut-shaped core includes 9 subunits that associate with the 3′ to 5′ exoribonucleases Rrp6, and Rrp44/Dis3, a subunit that also catalyzes endoribonuclease activity. Although recent structures and biochemical studies of RNA bound exosomes from *S. cerevisiae* revealed that the Exo9 central channel guides RNA to either Rrp6 or Rrp44 using partially overlapping and mutually exclusive paths, several issues related to RNA recruitment remain. Here, we identify activities for the highly basic Rrp6 C-terminal tail that we term the 'lasso' because it binds RNA and stimulates ribonuclease activities associated with Rrp44 and Rrp6 within the 11-subunit nuclear exosome. Stimulation is dependent on the Exo9 central channel, and the lasso contributes to degradation and processing activities of exosome substrates in vitro and in vivo. Finally, we present evidence that the Rrp6 lasso may be a conserved feature of the eukaryotic RNA exosome.

INTRODUCTION

The eukaryotic RNA exosome is a conserved multi-subunit protein complex involved in RNA turnover, processing, maturation and quality control (1,2). Its RNA targets are broad and diverse, ranging from normal mRNA turnover in the cytoplasm, to nuclear functions that encompass processing of ribosomal RNA, snoRNAs and snRNAs, to decay of aberrant tRNAs, mRNAs and noncoding RNAs such as cryptic unstable transcripts (CUTs) that arise from bidirectional transcription (3–11). Its core consists of a catalytically inert scaffold of nine essential and distinct subunits (Exo9), that together form a two-stacked ring of approximately 300 kilodaltons (kDa), with six RNase PH-like proteins on the bottom (Rrp41, Rrp45, Rrp46, Rrp43, Rrp42, Mtr3), and three S1/KH domain 'cap' proteins on the top (Csl4, Rrp4, Rrp40) (12). A prominent central channel is located at the center of the ring. The channel is essential *in vivo* (13), where it guides single stranded RNA to the catalytic subunits of the cytoplasmic and nuclear RNA exosome.

The Exo9 core associates with one or two ribonucleases that catalyze 3′ to 5′ exoribonuclease and endoribonuclease activities. In *Saccharomyces cerevisiae*, the Exo9 core interacts with Rrp44, alternatively referred to as Dis3, to form a 10-subunit exosome in the cytoplasm ($Exo10^{44}$), and with Rrp6 and Rrp44 to form an 11-subunit exosome in the nucleus ($Exo11^{44/6}$). Rrp44 is a processive 3′ to 5′ exoribonuclease, and a member of the RNase II/R family (14). Like bacterial RNase II/R, its active site is located in the RNB domain, and is flanked by one S1 domain and two cold shock domains (CSDs). Rrp44 also catalyzes endoribonuclease activity via an active site located in its N-terminal PIN domain (15–17). While Rrp44 is an essential gene, its endo- or exoribonuclease activities are not essential, although mutation of both active sites results in synthetic lethality (15–17).

Rrp6 catalyzes distributive 3′ to 5′ exoribonuclease activity and is a member of the RNase D family (18). Yeast Rrp6 includes 733 residues and at least four distinct functional domains. The N-terminal PMC2NT domain binds to a protein cofactor, Rrp47, which is necessary for Rrp6 stability in vivo where it assists in recruitment of the TRAMP complex (19–21). The EXO domain contains the 3′ to 5′ exoribonuclease active site, however both the EXO and HRDC domains constitute the Rrp6 catalytic module (CAT). The C-terminal domain (CTD) includes approximately two hundred residues. The Rrp6 CTD is apparently unstructured when not associated with the exosome but amino acids 518–616 adopt structure when associated with Exo9 through contacts to Csl4, Rrp43 and Mtr3 (22–24), forming the Rrp6 Exosome Associating Region or EAR domain. The remaining 100 amino acids of the Rrp6 CTD contains a putative nuclear localization sequence (pNLS), however other functions for this region have escaped notice as its alteration does not lead to mislocalization or apparent growth phe-

*To whom correspondence should be addressed. Tel: +1 212 639 8205; Fax: +1 212 717 3047; Email: limac@mskcc.org

notypes (25). Furthermore, this region of the Rrp6 CTD is either not present or disordered in all available structures as no electron density was observed beyond amino acid 621 (22–24). Although formal proof is lacking, the lack of conserved secondary structure and amino acid composition suggest this region is likely disordered.

Recent crystal structures of yeast exosomes bound to Rrp44 (22) or Rrp6 (23) or both enzymes (24) bound to RNA revealed how the Exo9 core might contribute to their activities. In the structure of the Rrp44-bound exosome ($Exo10^{44/Rrp6EAR}$), Rrp44 is tethered to the bottom of the Exo9 PH-like ring via its PIN domain, with the RNB domain positioned below the central channel. If long enough, RNA passes through the central channel to bind Rrp44 (26). The EAR domain of the Rrp6 CTD (518-618) associates with Exo9. The structure of $Exo10^{6}$ bound to polyA RNA shows the Rrp6 EAR domain in the same position, while the catalytic module of Rrp6 rests atop the S1/KH ring, with its EXO domain located above the Exo9 central channel. Despite Rrp44 and Rrp6 occupying opposite ends of the Exo9 core, both catalytic subunits' exoribonuclease and endoribonuclease activities are dependent on the integrity of the Exo9 central channel which guides RNA into each active site, and in turn modulates the activities of all three ribonuclease activities (13,27).

These structures provided insights to RNA degradation by the exosome with RNA substrates bound to the active sites (mutated to prevent hydrolysis); however insights to other functional domains required for earlier steps—such as RNA binding, and subsequent path selection through Exo9 to Rrp6 or Rrp44, remain less clear. Furthermore, a role for the last 100 amino acids of the Rrp6 CTD in RNA processing and/or decay has not been addressed. Here, we show that the last one hundred residues of Rrp6 can function as a RNA recruitment factor, which we refer to as the RNA 'lasso'. In the case of free Rrp6, the lasso can enhance RNA decay, presumably through addition of another RNA binding surface. In association with the Exo9 core, the lasso can stimulate each of the known activities of the nuclear RNA exosome in a process that is dependent on the length of the RNA substrate.

MATERIALS AND METHODS

Exosome subunit purification, complex reconstitution and analyses

Expression and purification of recombinant exosome subunits and subsequent complex reconstitution were performed as described previously (13,23,28). Unless otherwise noted, all constructs were cloned into pRSF-Duet1 with His_6-Smt3 cloned into MCSI to generate exosome subunits with cleavable N-terminal Smt3 tags, and expressed in *Escherichia coli* BL21 (DE3) RIL. Point mutations in the core subunits Mtr3 K132E, Rrp4 W278A and Csl4 R206D were introduced by PCR-based mutagenesis. Smt3-Rrp6 CAT fused to Csl4 by a 9 residue exogenous linker was generated by PCR by amplifying the Rrp6 coding region corresponding to residues 128–518, incorporating DNA encoding the sequence TGSTGSTGS, followed by Csl4. Constructs with the Rrp6 lasso fused to the Csl4 C-terminus either encoded DNA corresponding to *Saccharomyces cerevisiae* Rrp6 618–733, 685–733, or *Homo sapiens* 741–885. His_6-GST-Rrp6 CTD (residues 518–733) was cloned into pET28b bearing a His_6-GST fusion with a TEV cleavage site, expressed using LB, and induced with 0.4 mM IPTG at 18°C overnight. Cleared cell lysates were loaded on a nickel-NTA column. Nickel eluates were further purified via size exclusion chromatography (Superdex 200), and a final heparin column to remove contaminating nucleic acid and to separate degradation products. His_6-Smt3-Rrp6 618–733 was expressed and similarly purified except that eluates from nickel-NTA were loaded on a Superdex 75 column, followed by cleavage with Ulp1, and the cleaved products and contaminating nucleic acid separated on a heparin column. Wild-type and catalytically dead (D238N) Rrp6 lacking the Exosome Associating Region (EARless, corresponding to residues 128–516,618-733; and 128–516,618-685) or lasso (Lassoless minus or plus NLS, corresponding to residues 128–634, and 128–634, 700-721; or Partial Lasso, corresponding to residues 128–685) were expressed in 4 liters of Superbroth (Teknova), and purified by nickel affinity chromatography, and gel filtration (Superdex 200). All constructs were verified by DNA sequencing.

Analytical gel filtration studies were conducted by preincubating 150 micrograms of Exo9 with 2-fold molar excess of either Rrp6 128–733 (lasso intact); 128–634 (lassoless) or 128–516; 618–733 (EARless) on ice for 1 h. Samples were run on a Superose 6 and fractions analyzed by SDS-PAGE and visualized with Sypro Ruby.

Limited proteolysis experiments used 8 micrograms of $Exo10^{6exo-}$ incubated with chymotrypsin at 300, 100, 30, 10, 3.7, 1.2, 0.4, 0.14 or 0.05 ng. After one hour incubation at room temperature in 100 mM NaCl, 20 mM Tris pH 8.0, 10 mM DTT, 0.5 mM $MgCl_2$, reactions were quenched with LDS sample buffer, boiled for 2 min at 95°C, and analyzed by SDS-PAGE. For reactions containing RNA, $Exo10^{6exo-}$ was incubated with 3-fold molar excess of 36 nt AU-rich RNA on ice for 20 minutes prior to addition of chymotrypsin.

RNA degradation assays

RNA oligonucleotides were synthesized with a 5′ fluorescein as described previously (13,29) and purchased from IDT or Dharmacon, with the exception of $tRNA_{iMet}$. 5′ fluorescein labeled ssRNAs used in this study included AU-rich RNAs of 14, 18, 24, 36 and 49 nts with sequence AUU UAU UUA UUA UU; AUU AUU UAU UUA UUU A UU; AUU AUU UAU UUA UUA UUA UUU AUU; AUU AUU UAU UUA UUA AUU AUU UAU AUU UUA UUU AUU; AAU UAU UUA UUA UUU AUU UAU UAU UUA UUU AUU UAU UAU UUA UUU AUU A. 5′ fluorescein-labeled generic stem loop RNA with a 3′ 9 nt single-stranded extension was described and characterized previously (29). 5′ fluorescein-labeled $tRNA_{iMet}$ stem loop corresponds to the acceptor stem and has the sequence AGC GCC GGA GAC GGC GCU ACC A. *S. cerevisiae* $tRNA_{iMet}$ was cloned into pHG300, *in vitro* transcribed, and purified by denaturing PAGE according to previously published protocols (30,31), and 5′ end labeled with fluorescein (32).

Unless otherwise noted, exoribonuclease assays were performed under multiple turnover conditions with 1 nM enzyme and 10 nM RNA. Experiments assaying cooperativity between the S1/KH domain of Exo9 and the Rrp6 lasso, and Exo10$^{6\text{-}3X}$ and the Rrp6 lasso utilized 2.5 nM enzyme and 10 nM RNA. Exoribonuclease assays were conducted in 50 mM KCl, 20 mM Tris–HCl (pH8.0), 10 mM DTT, 0.5 mM $MgCl_2$, and 1U/μL RNase inhibitor (NEB) at 30°C, as described previously (13,23). RNA intermediates were resolved by denaturing PAGE and visualized with a Fuji FLA-5000 fluoroimager. To quantify Rrp44 exoribonuclease activity, the fraction of full-length RNA degraded at a given time was calculated (13). Rrp6 exoribonuclease activity was quantified by dividing the median length of the RNA intermediates at a given time by the full-length RNA substrate to determine the fraction of RNA remaining (13). For both activities, data from triplicate experiments were analyzed using GraphPad Prism 6, and initial rates were calculated from data obtained within the linear range. For Exo10^6, data were fit to either one-phase or two-phase decay models, and the best fitting model selected by the extra sum-of-squares F test, with a *P* value cutoff of 0.05.

Endoribonuclease assays utilized variants of Rrp44 and Rrp6 that contained mutations in their respective active sites (Rrp44 D551N and Rrp6 D238N). Assays were carried out in the same reaction buffer used for exoribonuclease activity except 3 mM $MnCl_2$ was added to initiate the assays, with 10 nM protein and 10 nM 5′ fluorescein-labeled RNA.

RNA binding by fluorescence polarization

Fluorescence polarization experiments were performed by pre-incubating 50 nM 5′ fluorescein labeled RNA (14 nt, 18 nt, 24 nt, 36 nt AU-rich and 8 nt, 14 nt, and 37 nt polyA) on ice with increasing concentrations (0–6000 nM) of proteins or complexes that harbored exoribonuclease dead mutations in Rrp44 or Rrp6. The binding buffer consisted of 50 mM KCl, 20 mM Tris (pH 8.0), 10 mM DTT, 0.5 mM $MgCl_2$ and 0.1% NP-40. Fluorescence polarization measurements were carried out as described previously (13). Using data from triplicate experiments, a model for receptor depletion was used to calculate apparent K_d values with Prism, GraphPad Software.

Yeast growth assays

The *rrp6Δ* strain in the W303 background was a gift from Michael Rosbash (33). For *rrp6Δ*, haploid strains were transformed with a *CEN URA3* (pRS416) plasmid bearing wild-type *RRP6*, or *rrp6* alleles containing deletions in the NTD, lasso or EAR, or vector alone, under control of the *RRP6* endogenous 5′ and 3′ UTRs. Strains bearing pRS416 plasmids were selected after transformation by plating on minimal media (SD-Ura). Loss of the respective *CEN URA3* plasmid was selected for by plating on SD+5-FOA. Growth was monitored at 23°C, 30°C, and 37°C over a period of 10 days. No discernable phenotype was apparent at 23°C so growth experiments were conducted at 30°C and 37°C. The *rrp44Δrrp6Δ* strain in the S288C background (*MATa*, *his3Δ*, *leu2Δ*, *ura3Δ*, *rrp44*::*HYG rrp6*::*NEO* [*RRP44*, *URA3*] [*RRP44 D551N*, *LEU2*] was a gift from Ambro van Hoof. Strains were similarly transformed with a *CEN HIS3* (pRS413) plasmid bearing wild-type *RRP6*, or *rrp6* alleles containing vector alone or lasso deletions, and selected on SD-His-Leu-Ura. For the spotting assays, serial 10-fold dilutions (starting at OD_{600} of 1) of liquid cultures grown in selective minimal media were spotted on solid agar. For the W303 strains, yeast were spotted on composed of minimal (SD-Ura) or rich (YPAD) media supplemented with 200 μg/ml geneticin and grown at 30°C and 37°C. For the S288C strains, yeast were spotted on minimal media, in the absence (SD-Ura-Leu-His) and presence of 5-FOA (SD-Leu-His+5-FOA) and grown at 30°C and 37°C. For the W303 strains, liquid cultures of the transformants were grown at 37°C in minimal and rich media supplemented with 200 μg/ml geneticin.

Rrp6 protein expression was confirmed by Western blot using an affinity-purified polyclonal antibody raised against the yeast Rrp6 catalytic domain (residues 128–518) (Pocono Rabbit Farms). Ten to 20 micrograms of native whole cell lysates were probed with 1:3000 of anti-Rrp6, and 1:6000 anti-rabbit IgG HRP (GE).

RNA analyses from yeast

Nucleic acid-free His_6-GST-Rrp6 CTD (residues 518–733) or buffer was incubated in yeast whole lysate derived from *Δrrp6*, and then pulled down with nickel-NTA beads. To distinguish between nucleic acid bound to His_6-GST and the Rrp6 CTD, eluates were treated with TEV protease, and reapplied to nickel NTA-beads. Eluates were treated with either RNase A or DNase I, followed by Proteinase K digestion, and analyzed by denaturing (urea) PAGE. Nucleic acid was visualized with Sybr Gold.

For analysis of exosome substrates by qPCR, yeast strains were grown in 10 ml YPAD at 30°C until A_{600} 0.8, and were collected by centrifugation. Isolation of total RNA, reverse transcription, and analysis of cDNA by qPCR were performed using protocols and oligonucleotides described previously (13). PCR reactions were performed in triplicate, with scR1 mRNA used for normalization. RNA target levels are represented as fold enrichment over wild-type, with one-way ANOVA tests performed using GraphPad Prism 6.

RESULTS

Rrp6 CTD includes a functional domain that binds RNA

As noted above, the presumably unstructured Rrp6 CTD encompasses amino acid residues 518–733. Amino acids 518–616 adopt structure when associated with Exo9 through contacts to Csl4, Rrp43 and Mtr3 (22–24), forming the Rrp6 EAR. Consistent with the remaining portion being disordered, the CTD residues are vulnerable to proteolysis by chymotrypsin, in the absence and presence of RNA, while the rest of the Rrp6 exosome, including the EAR, is resistant (Supplementary Figure S1A). Sequence analysis of residues 634–733 reveals clusters of lysine and arginine residues, and a calculated isoelectric point of 10.3. Although this region shows poor sequence conservation (Figure 1A, Supplementary Figure S2), its physiochemical prop-

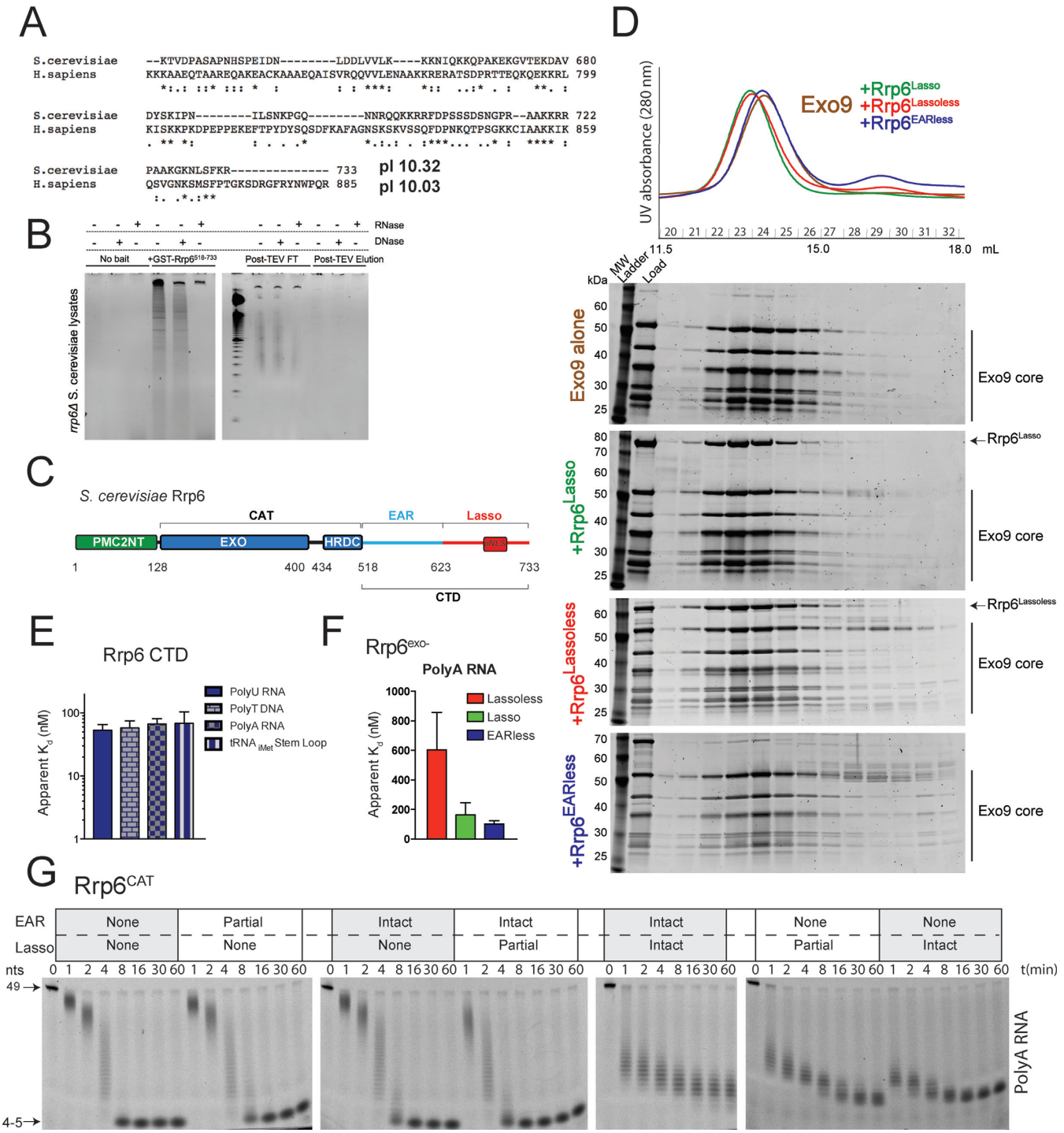

Figure 1. The Rrp6 CTD is composed of two modules—an Exosome Associating Region (EAR) and a 'lasso' that binds RNA and facilitates RNA decay. (**A**) The C-terminal most 100 residues of *S. cerevisiae* Rrp6 aligns poorly with that of *H. sapiens*, but both are highly basic with similar isoelectric points (pI). Alignments performed with ClustalW (58) and pI values calculated with Expasy Protparam (59). (**B**) Recombinant Rrp6 CTD (EAR and lasso) binds endogenous RNA from *S. cerevisiae* lysates. Representative denaturing PAGE stained with Sybr Gold is shown. (**C**) Revised domain structure of Rrp6. (**D**) Rrp6 association with Exo9 is dependent on the Rrp6 EAR, but independent of its lasso. Analytical gel filtration analyses and corresponding gels show Exo9 alone (brown); +Rrp6 with CTD intact (green); +Rrp6 lacking the lasso [Lassoless] (red); +Rrp6 lacking the EAR [EARless] (blue). (**E**) Fluorescence polarization binding measurements of the Rrp6 CTD on 5′ fluorescein-labeled 36 nt single-stranded polyU and polyA RNAs, polyT DNA, and 22 nt double-stranded $tRNA_{iMet}$ acceptor stem. (**F**) Catalytically dead Rrp6 variants (D238N) were analyzed for their ability to bind 37 nt polyA RNA via fluorescence polarization. Data shown as mean ± S.D. ($n = 3$ technical replicates). (**G**) Rrp6 ribonuclease activities on 5′ fluorescein labeled 49 nt single-stranded polyA RNA. Constructs vary from the Rrp6 minimal catalytic module to those containing a partial and intact EAR and lasso domains.

erties appear conserved (Supplementary Table S1).

The highly basic character of the Rrp6 CTD suggests it might bind nucleic acid. Indeed, recombinant His_6-GST-Rrp6-CTD interacts with nucleic acid from yeast lysates in a pull-down assay; and treatment with RNase A, but not DNase I, results in loss of most of the associated nucleic acid. Binding of RNA to the GST-Rrp6-CTD fusion appears dependent on the CTD as TEV cleavage released the Rrp6-CTD and RNA and because RNA was not retained in the His_6-GST elution (Figure 1B). Given its apparent disorder and ability to bind nucleic acid, we defined this region (amino acids 634–733) as the Rrp6 'lasso' (Figure 1C). To determine the extent of nucleic acid binding, dissociation constants were calculated for the Rrp6 CTD on various nucleic acids by fluorescence polarization. The Rrp6 CTD binds nucleic acid with a K_d of 50–60 nM, regardless of the nucleic acid type, using single-stranded RNA or DNA, or structured RNA (Figure 1E), while the Rrp6 lasso (residues 618–733) binds polyA RNA with an approximate K_d of 1 nM, at least 5-fold tighter, as we were at the detection limits of the assay (Supplementary Figure S1B).

We next queried if the Rrp6 lasso and EAR contribute to activities as distinct functional domains. Exosomes were reconstituted with different Rrp6 constructs including or lacking the lasso or EAR and evaluated for complex formation via size exclusion chromatography. Consistent with previous studies (13,23), Rrp6 containing the EAR and lasso reconstitute as a 1:1 complex with Exo9. Rrp6 that contains the EAR, but that lacks the lasso (Lassoless), also associates with Exo9. In contrast, Rrp6 lacking the EAR and containing the lasso (EARless) no longer associates with Exo9 (Figure 1D). These results are consistent with available structures and suggest the existence of two distinct elements within the C-terminal two hundred residues of Rrp6, the EAR and lasso.

We next determined the effects of disrupting the Rrp6 EAR and lasso on Rrp6 exoribonuclease activity. All constructs lacked the PMC2NT domain as it was shown previously that deletion of this region does not alter Rrp6 activity in comparison to full-length Rrp6 *in vitro* (13). Consistent with the lasso's ability to bind RNA (Figure 1E), lasso-containing Rrp6 binds single-stranded polyA RNA 4-fold better than lassoless Rrp6 (Figure 1F). Interestingly, EARless Rrp6 has the highest affinity for RNA, binding 6-fold better than its lassoless counterpart. This construct also degrades polyA RNA, a model substrate for the nuclear exosome (34), more efficiently than the catalytic module (Figure 1G). These results suggest that the EAR, when not bound to Exo9, slightly inhibits Rrp6 catalytic activity.

Degradation of polyA RNA is comparable when assaying activities of the Rrp6 catalytic module (EXO and HRDC domains, residues 128–516) with and without varying lengths of the EAR (residues 128–589; 128–634). However, a construct containing a partial lasso sequence (residues 128–685) results in a modest increase in RNA decay activity, while an intact lasso confers the highest activity (Figure 1G). These trends are also evident using an AU-rich RNA substrate (Supplementary Figure S1C and D). While the lasso enhances RNA decay by Rrp6, degradation results in larger RNA intermediates that accumulate at ∼9–12 nucleotides, rather than ∼4–5 nucleotides as observed for lassoless Rrp6 constructs (Supplementary Figure S1E). The larger product distributions do not appear to be due to enzyme instability, as similar trends are observed for RNA substrates shorter than 49 nucleotides. Furthermore, the Rrp6 CTD is not sufficient to generate larger products when added to the catalytic module in trans (Supplementary Figure S1F). EARless Rrp6 does not accumulate larger products when compared to full-length Rrp6 (Figure 1G). The mechanism underlying differences in product lengths is not clear, but two possibilities are that the EAR inhibits Rrp6 or that the Rrp6 lasso inhibits further degradation of RNA to 4–5 nt because it binds RNA, preventing further association with the Rrp6 active site, especially when linked via the EAR domain. The data presented thus far suggests that the lasso can enhance degradation of single-stranded RNAs by free Rrp6.

The lasso binds RNA and stimulates Rrp6 and Rrp44 activities in exosomes

We next determined if the lasso could stimulate Rrp6 activities when associated with the exosome core. Three Rrp6 constructs were reconstituted and purified with recombinant Exo9 including those containing full-length lasso (128–733), partial lasso (128–685) and lassoless (128–634). Each were assayed for degradation using AU-rich and polyA RNA. In this context, the lasso had a more pronounced effect on $Exo10^6$ than observed for free Rrp6 (Supplementary Figure S3A). With AU-rich RNA, partial or full lasso deletion results in a 9-fold and 25-fold loss of Rrp6 activity, respectively, compared to full-length lasso. Similar trends are observed for polyA RNA, with partial and full lasso deletions resulting in 4-fold and 14-fold less decay (Figure 2A).

Rrp6 association with the Exo9 core modulates Rrp6 activities, generating a tighter distribution of RNA products compared to the broad distribution of products observed for free Rrp6 (13). RNA intermediates of exosomes that include Rrp6 with an intact lasso reveal this tight distribution, whereas exosomes containing partial and lassoless Rrp6 produce a broader distribution of products that is more similar to free Rrp6 (Figure 2A and B). We posit that disparities in product distributions could be due to differences in binding affinities for RNA within various exosomes, with the lasso contributing to RNA binding. Indeed, a 20-fold loss of binding to AU-rich RNA was observed for exosomes lacking an intact lasso (Supplementary Figure S3C), and >15-fold loss for polyA RNA binding, a conservative estimate given that polyA RNA binding could not be saturated for partial- or lassoless $Exo10^6$ (Figure 2C).

Rrp6 stimulates Rrp44 ribonuclease activities in $Exo11^{44/6}$, an effect that is dependent on the Rrp6 catalytic module and CTD but independent of Rrp6 catalytic activity and PMC2NT domain (13,23). To determine if the lasso alters Rrp44 activities, $Exo11^{44/6}$ was reconstituted using Rrp6 full lasso, partial lasso, and lassoless, in the context of catalytically active and catalytically inactive Rrp6. Partial or complete removal of the Rrp6 lasso in $Exo11^{44/6Partial}$ or $Exo11^{44/6Lassoless}$ compromised Rrp44 activity in degradation of polyA RNA, down 4-fold and 14-fold, respectively (Figure 2B). This trend appears independent of Rrp6

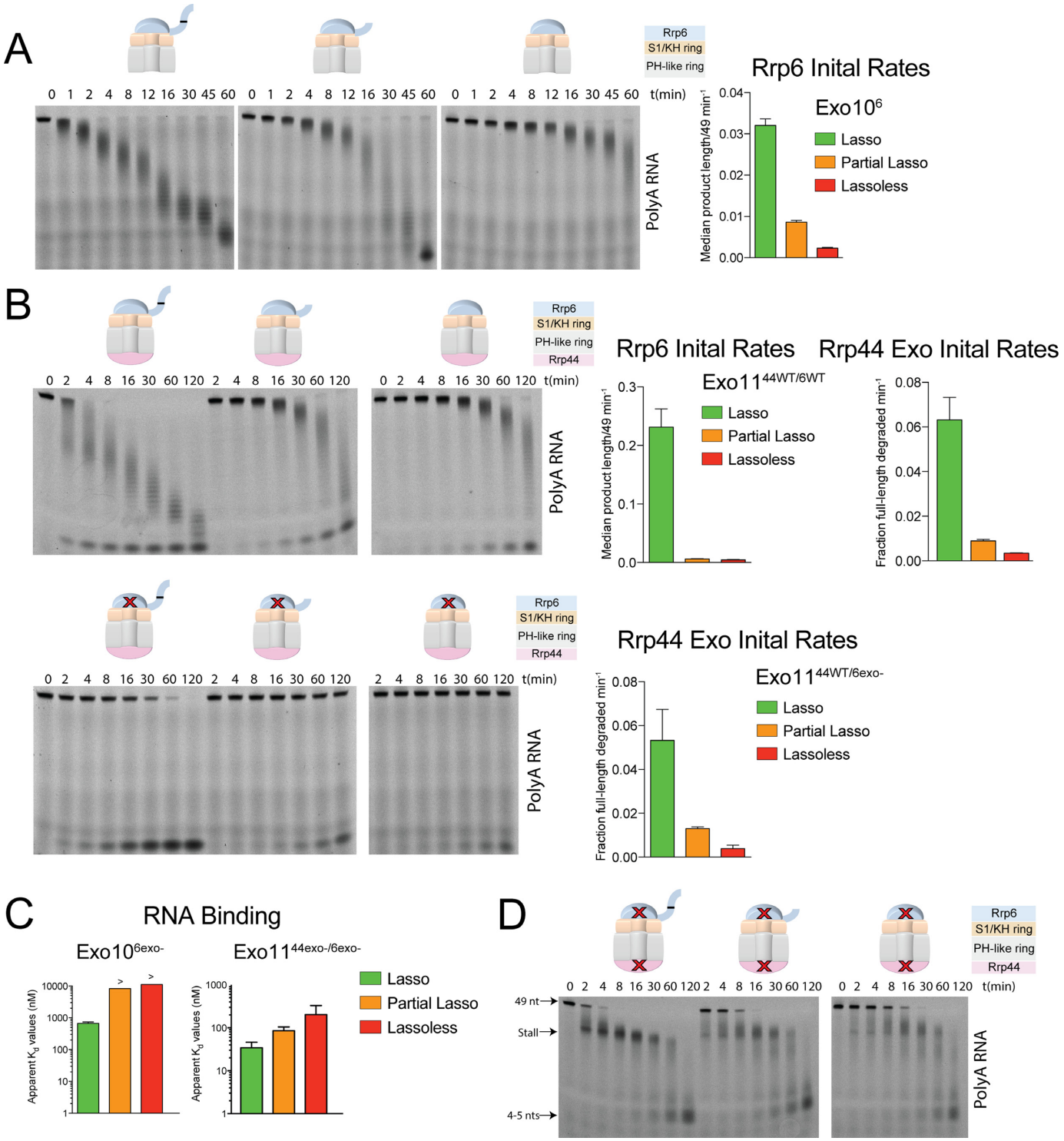

Figure 2. The Rrp6 lasso stimulates all three ribonuclease activities of the exosome. (**A**) Rrp6 activity on 49 nt polyA RNA is diminished when the lasso is compromised in the context of Exo10^{6}. Rrp6 rates are shown as mean ± S.D. ($n = 3$ technical replicates). (**B**) Rrp6 and Rrp44 exoribonuclease activities on 49 nt polyA RNA are attenuated by lasso deletions in Exo11$^{44/6}$ and Exo11$^{44/6exo-}$. Bar graphs depict initial rates of Rrp44 and Rrp6 exoribonuclease activities, shown as mean ± S.D. ($n = 3$ technical replicates). (**C**) Catalytically dead Rrp6 (D238N) and Rrp44 (D551N) variants of Exo10^{6} and Exo11$^{44/6}$ with different lasso lengths were analyzed for their ability to bind 37 nt polyA RNA via fluorescence polarization. Data shown as mean ± S.D. ($n = 3$ technical replicates). (**D**) Endoribonuclease activity of Rrp44 on 49 nt polyA RNA is altered by Rrp6 lasso deletion.

catalytic activity (Figure 2B). Although Rrp44 readily degrades AU-rich RNA in both 10- and 11-subunit exosomes, Exo11$^{44/6Lasso}$ Rrp44 degrades RNA 13-fold more efficiently than Exo11$^{44/6Partial}$ and Exo11$^{44/6Lassoless}$ (Supplementary Figure S3B). Furthermore, RNA binding of Exo11$^{44exo-/6exo-}$ is compromised by lasso deletion, leading to a 6-fold decrease in affinity for polyA RNA (Figure 2C). The presence of Rrp44 in Exo11$^{44/6}$ did not alter the effects of the lasso, or lack thereof, on Rrp6 activities as observed for Exo10^{6} (Figure 2B, Supplementary Figure S3B). It is important to note that the Rrp6 CTD (including the EAR and lasso) is not sufficient to stimulate Rrp44, suggesting that the Rrp6 catalytic module is also needed, perhaps by widening the central channel to enhance RNA ingress through Exo9 to gain access to the Rrp44 active sites (23).

We next assessed if the Rrp6 lasso alters Rrp44 endoribonuclease activity. Rrp6, again independent of its catalytic activity, stimulates the Rrp44 endoribonuclease activity in Exo11$^{44/6}$ (Figure 2D). Endoribonuclease activity of free Rrp44 appears distributive with little or no directionality detected in cleavage intermediates (15,16). In contrast, Exo9 association with Rrp44 converts the endoribonuclease activity to a 3′ to 5′ directionality on AU-rich RNA where it generates a 'footprint' that is dependent on the integrity of the Exo9 central channel (13) (Supplementary Figure S3D). The endoribonuclease 'footprint' for polyA RNA also requires Rrp6 association in Exo11$^{44/6}$, and is more pronounced in the presence of the Rrp6 catalytic module (23) and lasso (Figure 2D).

The Rrp6 lasso is more important for degrading longer RNA

Degradation of 49 nucleotide single-stranded RNA by Exo10^{6Lasso} generates a tighter distribution of intermediates and a higher initial rate than observed for partial and lassoless Exo10^{6} (Figure 2A, Supplementary Figure S3A). This decay pattern can be modeled as biphasic, with a rapid initial phase, followed by a slower second phase, an effect not observed when using shorter RNAs. In contrast, Exo10^{6Partial} and Exo10^{6Lassoless} exosome activities are better modeled as a single-phase, in which longer and shorter RNAs behave similarly (Figure 3A).

Given these observations, we hypothesized that the lasso might exert differential effects on decay rates in an RNA length-dependent manner. Exo10^{6} was assessed for decay activity using 49, 36, 24, 18 and 14 nucleotide single-stranded RNAs in complexes containing intact, partial, and no lassos (Figure 3A and B, Supplementary Figure S4A). Lasso-containing exosomes degrade longer RNAs most efficiently while exhibiting the two-phase model for decay, with rates approximately 25-fold and 10-fold higher than lassoless exosomes on 49 and 36 nucleotide RNAs, respectively. Interestingly, activities change to a one-phase decay model when exosomes are offered RNA substrates 18 nucleotides and shorter, similar to mutants lacking the lasso. Although most of the RNA was not visible in the Exo10^{6}-polyA RNA structure, 24 nucleotides were required to obtain crystals with RNA bound in the Rrp6 active site (23). A more recent structure of a yeast nuclear exosome complex crystallized with a 18 nucleotide AU-rich RNA proposed an RNA path that bypasses the Rrp6 active site (24). While it is only possible to speculate, RNA substrates longer than 24 nucleotides may be better substrates for Exo10^{6Lasso} because they are long enough to span the binding surfaces between the Rrp6 active site, Exo9 S1/KH ring, and Rrp6 lasso, while shorter RNAs are unable to engage the lasso, are less stably associated, and less readily degraded. Consistent with this hypothesis, Exo10^{6Lasso} binds 24 nucleotide RNA the tightest, and exhibits lower affinities for 18 and 14 nucleotide RNA (Figure 3C). This trend holds for Exo10^{6Lassoless} although binding is weaker overall. It remains unclear why the 36mer RNA binds less well given the observed activities, but if 24 nucleotides represents an optimal length, there could be an entropic disadvantage to binding RNAs longer than 24 nucleotides in this assay.

An intact Rrp6 lasso promotes degradation of longer single-stranded RNAs, so we next tested if the lasso influences degradation of a hypomodified tRNA$_{iMet}$, a structured RNA and substrate of the nuclear exosome (35,36). Exo11$^{44/6}$ degrades 95% of this RNA (Figure 3D), generating intermediates, presumably at domains of more stable tertiary structure (Figure 3E, Supplementary Figure S4B), while 5% appears to be trimmed through the 3′ ssRNA extension and not degraded. In comparison, Exo11$^{44/6}$ was unable to degrade the majority of tRNA$_{iMet}$ beyond trimming of the 3′ ssRNA extension when the lasso was missing. To determine if the lasso stimulates activity on another structured RNA, a generic stem loop RNA bearing a 19 nt stem loop and 8 nt single-stranded 3′ extension (29) was used. Although this RNA could not be degraded beyond its 3′ ssRNA extension (Supplementary Figure S4C), the lasso confers a 3.5-fold advantage in degrading the single-stranded extension to the presumed base of the stem loop.

The Rrp6 lasso is proximal to the Exo9 central channel

The importance of the exosome central channel in Rrp44- and Rrp6-mediated RNA decay is evident *in vitro* and *in vivo* (13,23,27,37). Exosome structures containing the Rrp6 EAR (22–24) indicate that the lasso would be proximal to the top of the S1/KH ring (Figure 5A). If RNA interacts with the lasso, RNA would be positioned above the S1/KH ring, perhaps en route to Rrp6 or through the Exo9 central channel to Rrp44. If true, exosomes lacking the lasso might display a greater dependence on the integrity of the Exo9 central channel. Exoribonuclease activities of Rrp6 in Exo10^{6} and Rrp6 and Rrp44 in Exo11$^{44/6}$ were assessed in lasso-containing exosomes. Consistent with previous results (23), a triple point mutation in Rrp40 within the S1/KH ring results in slight inhibition of Rrp6 and Rrp44 activities, with greater inhibition observed when combined with three point mutations in Csl4 (Figure 4, Supplementary Figure S5). Exosomes with compromised lassos (either partial or lassoless) are less active in the presence of S1/KH mutations when compared to those containing intact lassos, while lasso compromised Exo10^{6} and Exo11$^{44/6}$ are less active on polyA RNA than intact exosomes in the presence of the Rrp40 triple mutant. Furthermore, lasso compromised Exo10^{6} appears less adept at degrading polyA or AU-rich RNA when combined with the Rrp40/Csl4 mutations (Supplementary Figure S5). These data suggest that the lasso

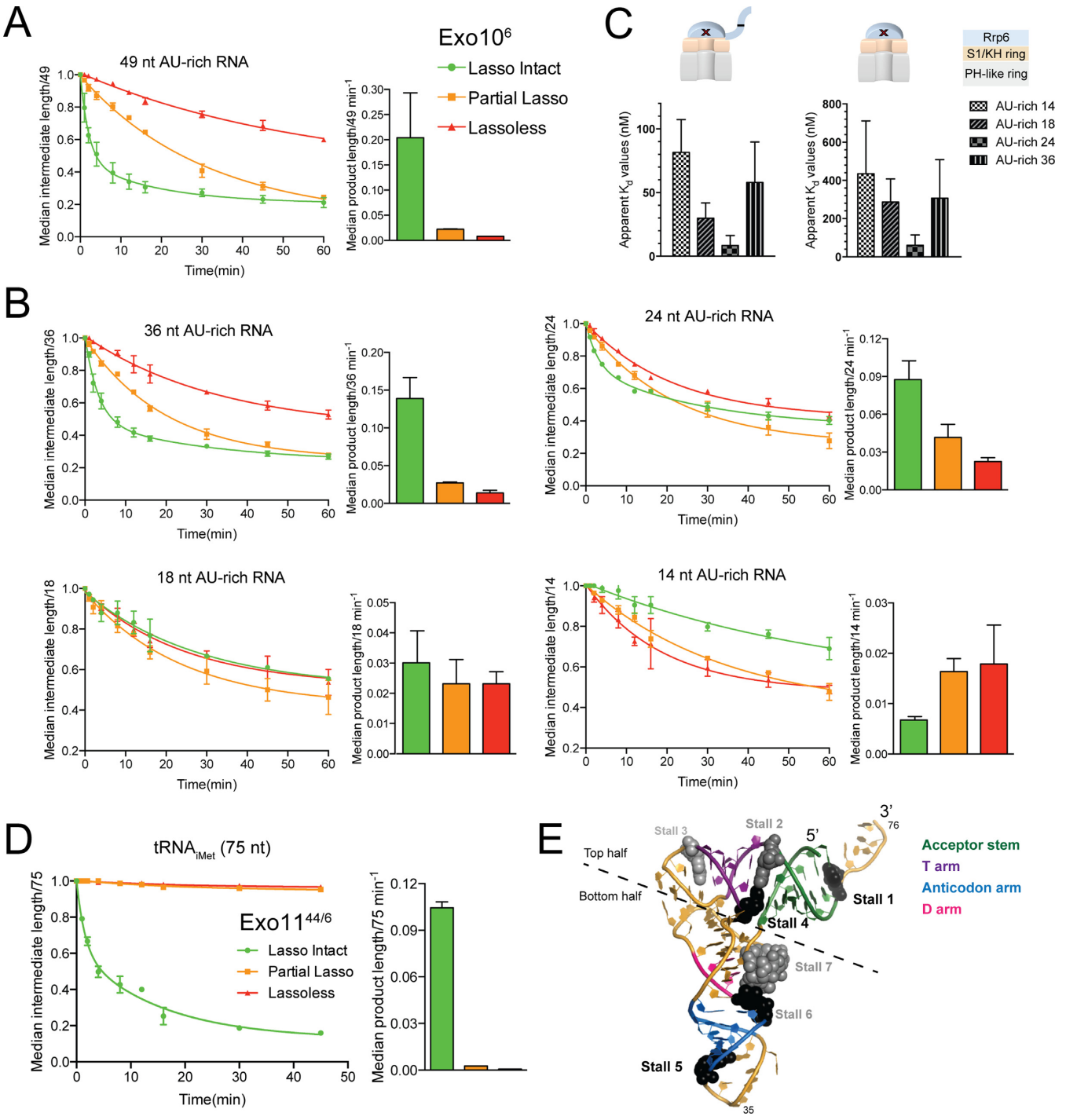

Figure 3. Stimulation by the Rrp6 lasso is dependent on RNA length. (**A**) Decay of 49 nt AU-rich RNA by Exo10^{6}, with and without the Rrp6 lasso. Exo10^{6Lasso} can be modeled as two-phase decay, while Exo10^{6Lassoless} follows a one-phase decay mechanism. Rrp6 rates are shown as mean ± S.D. (n = 3 technical replicates). (**B**) Different lasso variants of Exo10^{6} were assayed for their activities on 5′ fluorescein-labeled 36, 24, 18 and 14 nt single-stranded AU-rich RNAs. Bar graphs represented initial rates are shown as mean ± S.D. (n = 3 technical replicates). (**C**) 5′ fluorescein single-stranded 14, 18, 24 and 36 nt AU-rich RNAs were incubated with various concentrations of catalytically dead Exo10^{6Lasso} and Exo10^{6Lassoless} and binding measure by fluorescence polarization. Data shown as mean ± S.D. (n = 3 technical replicates). (**D**) Decay of 5′-fluorescein labeled hypomodified tRNA$_{iMet}$ by Exo11$^{44/6}$ with various lasso lengths. Rrp6 exoribonuclease activity is plotted as a function of time, and initial rates depicted as bar graphs representing mean ± S.D. (n = 3 technical replicates). (**E**) Crystal structure of tRNA$_{iMet}$ (PDB: 1YFG) color-coded according to domain, and Rrp6 predicted stall sites represented as spheres, with black and gray signifying major and minor stall sites, respectively. This and other structure figures were generated with PyMol (http://www.pymol.org).

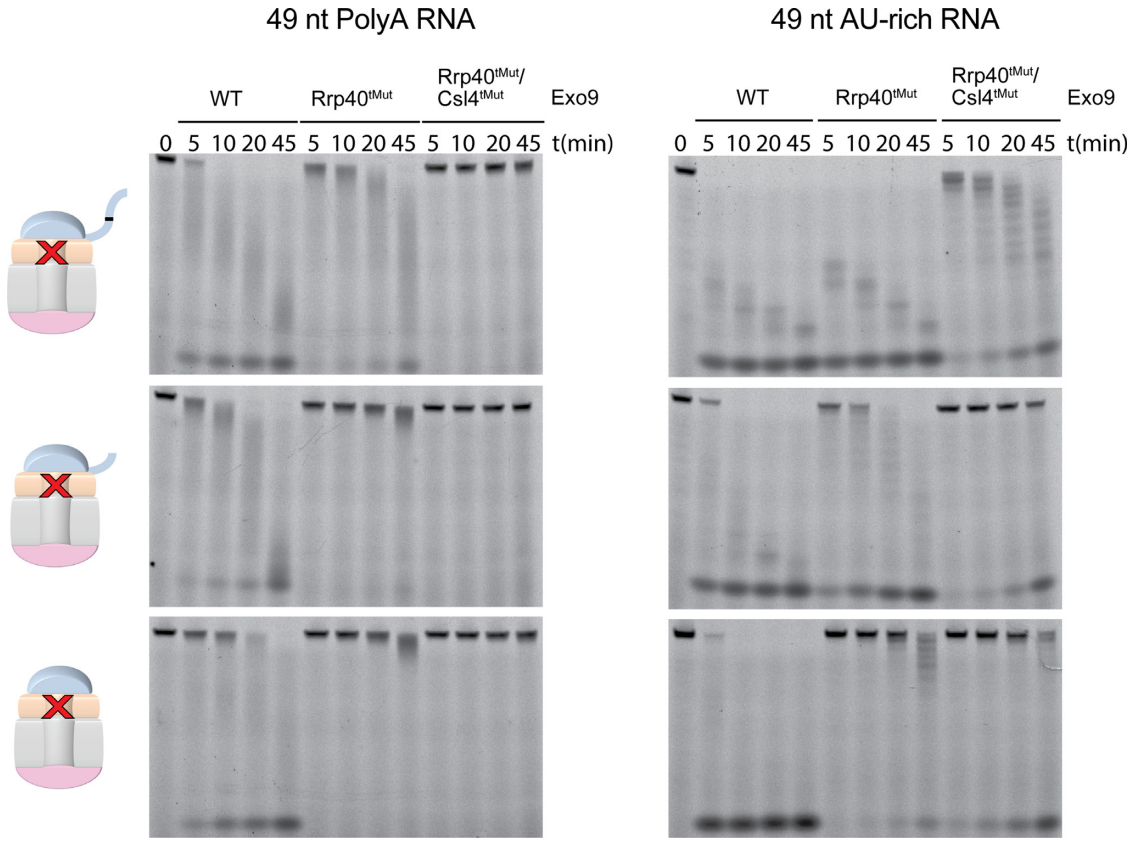

Figure 4. Stimulation by the Rrp6 lasso is dependent on the integrity of the Exo9 S1/KH ring in Exo11$^{44/6}$. Exo11$^{44/6}$ with different lasso lengths (intact, partial, and lassoless) with mutations within the S1/KH ring described previously (23) were assayed for their activities on 5′ fluorescein single-stranded 49 nt PolyA and AU-rich RNAs. Exo11$^{44/6}$ with lasso deletions are more sensitive to mutations within the S1/KH ring.

and central channel may cooperate to efficiently degrade RNA.

The EAR domain is dispensable for lasso stimulation of Rrp6 and Rrp44

The Rrp6 EAR is required for association with Exo9, so we engineered a variant of Rrp6 that associates with the exosome independent of the EAR. Using the structure of Exo10^{6} as a guide (23), the C-terminus of the Rrp6 catalytic module (residue 518) was fused to the N-terminus of the S1/KH subunit Csl4 via a nine-residue linker. Different Rrp6 lasso lengths were then fused to the Csl4 C-terminus, proximal to the location of the Rrp6 lasso in Rrp6-containing exosomes (Figure 5A). These engineered constructs, Rrp6^{CAT}-Csl4, Rrp6^{CAT}-Csl4-LassoPartial, and Rrp6^{CAT}-Csl4-LassoIntact were reconstituted with Exo10^{44} and assayed for activity alongside Exo10^{44} and Exo11$^{44/6}$. The lassoless Rrp6^{CAT}-Csl4 fusion exhibits diminished Rrp6 activity on both AU-rich and polyA RNA. In contrast, Rrp44 activity is stimulated on AU-rich RNA, although no effect is observed for polyA RNA (Figure 5B). These data suggest that the Rrp6 catalytic module is not sufficient for stimulation, but exosome complexes bearing Rrp6^{CAT}-Csl4 and lasso fusions to Csl4 resulted in activation of both Rrp44 and Rrp6 activities using AU-rich and polyA RNAs, with Exo11-Rrp6^{CAT}-Csl4-LassoPartial exhibiting activities comparable to wild-type Exo11$^{44/6}$. Although less active, the stimulatory effects of the lasso appear conserved as the C-terminal 144 residues of the putative *H. sapiens* lasso, when fused to *S. cerevisiae* Rrp6^{CAT}-Csl4, also stimulates Rrp44 and Rrp6 activities.

In vivo effects of lasso deletion

A previous study reported that Rrp6 CTD deletion rescued growth deficiencies associated with the *rrp6Δ* in *S. cerevisiae* in the S288C strain, although defects in the processing of some ribosomal RNA precursors, including 5′ ETS and 3′ truncated 5S RNAs, were noted (38). Because Rrp6-associated phenotypes are more pronounced in the W303 strain (39,40), we characterized Rrp6 lasso truncations in this background. We included residues 700–721 in each construct to maintain the putative nuclear localization sequence (pNLS), despite reports that mutating this region results in minimal mislocalization, no observable growth phenotype, and no accumulation of known Rrp6 and/or exosome targets (25). Interestingly, the pNLS appears to contribute in part to the stimulatory effects of the lasso as observed for Rrp44 and Rrp6 activities in reconstituted exosomes (Supplementary Figure S6A). Strains lacking *RRP6* were complemented with plasmids bearing no *RRP6*, full-length *RRP6* (1–733); *rrp6*-Δ635–699; 722–733 (lassoless), *rrp6*-Δ686–699; 722–733 (partial lasso); and *rrp6*-Δ519–

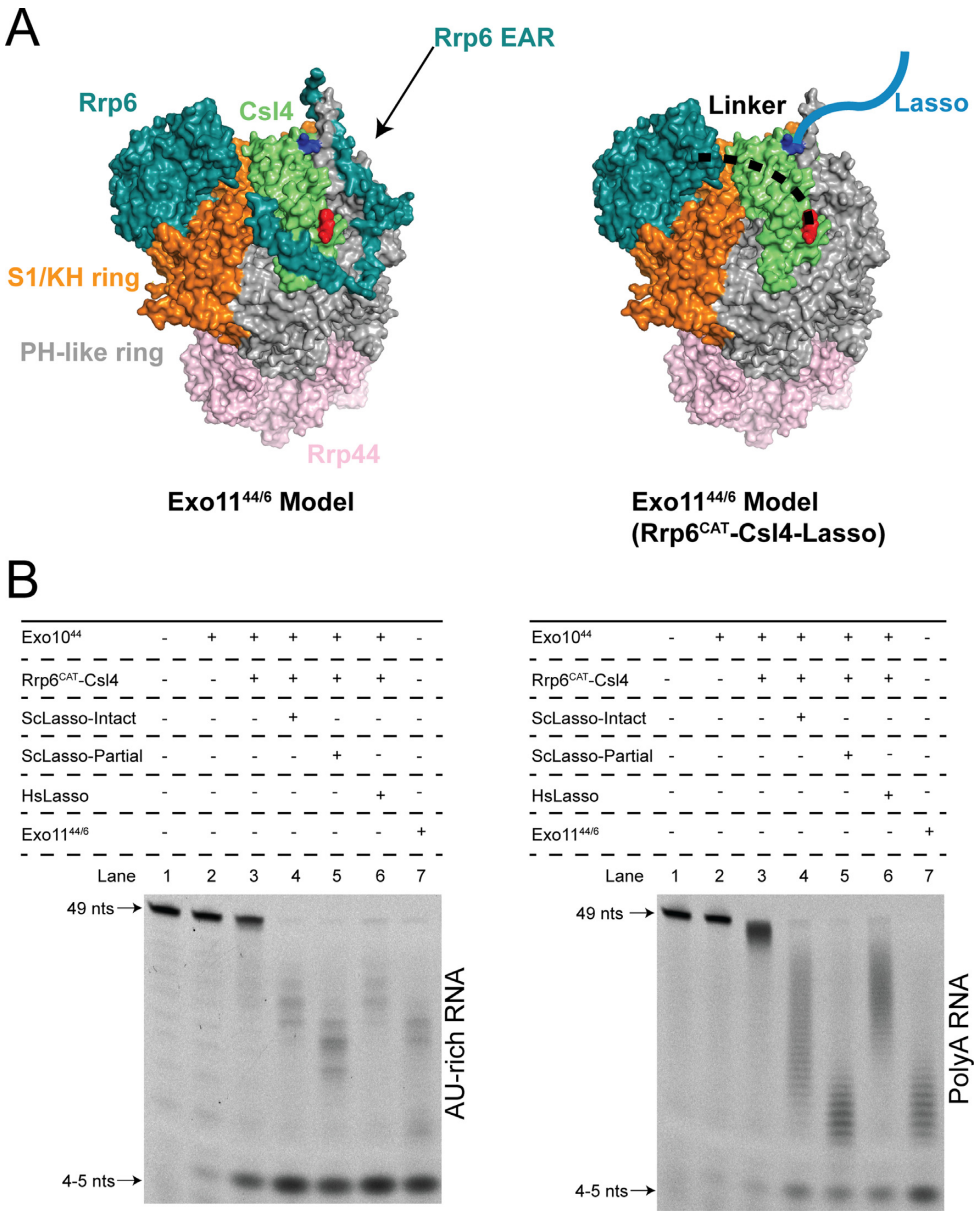

Figure 5. The Rrp6 lasso from human or yeast can stimulate Rrp6 and Rrp44 activities independent of the EAR. (**A**) Left: Model of Exo11$^{44/6}$ based on structure of Exo10^{6} (PDB: 4OO1) aligned to Rrp44 from Exo11$^{44/6CTD}$ (PDB: 4IFD). Right: Strategy for fusing the C-terminus of Rrp6-CAT to the N-terminus of Csl4 (red) to tether Rrp6-CAT to Exo9, bypassing the need for the Rrp6 EAR, and for appending variants of the Rrp6 lasso to the C-terminus of Csl4 (blue), proximal to the C-terminus of the Rrp6 EAR. Figure prepared with PyMol. (**B**) Endpoint decay (30 min for AU-rich; 60 min for polyA) of 5′ fluorescein labeled 49 nt AU-rich RNA (left) and polyA RNA (right) by various reconstituted exosomes under multiple turnover conditions. Rrp6$^{CAT-Csl4}$ signifies Exo10^{44WT} reconstituted with catalytically competent Rrp6$^{CAT-Csl4}$; ScLasso-Intact, ScLasso-Partial and HsLasso represent the same complex, but with the C-terminus of Csl4 bearing fusions of Rrp6 lasso residues 618–733, 685–733 from *S. cerevisiae*, and 741–885 from *H. sapiens*, respectively.

618 (EARless) and expression confirmed by western blot (Supplementary Figure S6C). Yeast grown in minimal media on solid agar (Figure 6A) or liquid media (Supplementary Figure S6B) exhibit very slight temperature sensitive growth defects for lassoless *rrp6* at 37°C. Growth in rich media exacerbates defects (Figure 6A, Supplementary Figure S6B). While EARless *rrp6* grew almost as well as wild-type *RRP6* on minimal media, it almost phenocopies *rrp6Δ* on rich media. It remains unclear if this is due to its inability to associate with Exo9 or if free EARless Rrp6 is hyperactive as noted above.

Several RNA substrates of the exosome known to be misregulated (7,9–10,13) in *rrp6Δ* strains were analyzed by quantitative PCR. The CUTs NEL025C and CUT273, accumulate slightly in strains harboring lasso deletions relative to those containing full-length *RRP6*, but not to the same extent as *rrp6Δ* or strains expressing EARless *rrp6* (Figure 6C). Processing of pre-ribosomal RNA within ITS2-1 is altered in strains lacking *RRP6* and other exosome subunits (5,13), and strains expressing lasso deletions exhibit levels of ITS2-1 comparable to the *rrp6Δ* strain, whereas EARless *rrp6* generates intermediate ITS2-

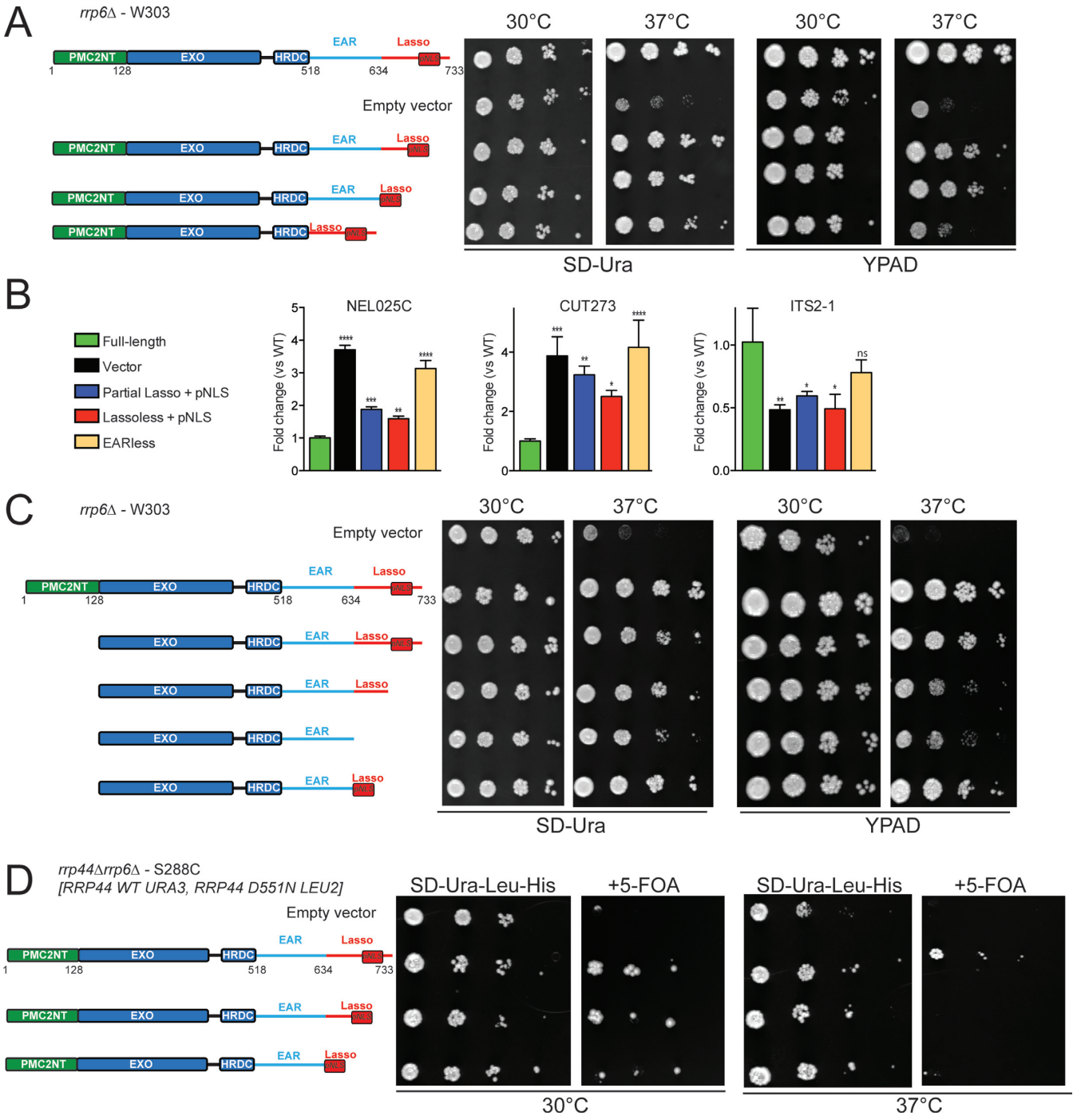

Figure 6. Analysis of the Rrp6 lasso in vivo. (**A**) *S. cerevisiae* W303 *rrp6Δ* complemented with lasso or EAR deletions exhibited more pronounced growth defects at 37°C on rich (right) rather than minimal (left) media when grown for two days on solid agar. (**B**) RNA abundance of known exosome substrates determined by qPCR from *rrp6* mutant strains grown in rich media at 30°C. Bar graphs represent fold-change over wild-type, mean ± s.d. (n = 3 technical replicates, **P* <0.05, ***P* <0.01, ****P* <0.001, *****P* <0.0001). Targets were normalized to *SCR1* mRNA. (**C**) Growth defects after two days at 37°C on rich media are exacerbated in when the Rrp6 PMC2NT and lasso are simultaneously deleted. Partial lasso restoration by addition of the pNLS partially restores the growth defect. (**D**) Rrp6 lasso deletions are synthetic with the Rrp44 D551N (exo-) mutation at 37°C. Growth on SD-Ura-Leu-His after three days, and on 5-FOA-Leu-His after 6 days.

1 levels between that observed for full-length RRP6 and *rrp6Δ*. While preliminary, these results suggest that defects observed for lasso compromised exosomes in vitro may have consequences in vivo, especially evident in rich media which differentially alters the transcriptome in comparison to minimal media (41). Indeed, alterations in exosome-dependent RNA metabolism in rich versus minimal media have been reported (20).

To query whether the growth defects present in lasso deletions are exacerbated when combined with mutations of other known exosome factors, we first combined the lasso mutants with deletion of the Rrp6 N-terminal PMC2NT domain. It is well established that deletion of this domain is coupled with loss of expression of the cofactor, Rrp47 (19,42), resulting in a slight growth defect when compared to full-length Rrp6 (43) (Figure 6C). Consistent with the lasso contributing to exosome activities, synthetic growth defects are observed on rich media at 37°C when deletions within the Rrp6 lasso and NTD are combined (Figure 6C). Interestingly, defects can be alleviated by addition of the putative NLS, despite similar expression levels (Supplementary Figure S6D). As a final test, Rrp6 lasso deletion mutants were combined with a Rrp44 exoribonuclease dead (D551N) mutant as this mutant results in synthetic lethality in the absence of Rrp6 (44). Indeed, Rrp6 lasso deletions fail to rescue the synthetic lethality of the Rrp44 D551N *rrp6Δ* at 37°C (Figure 6D), despite being expressed (Supplementary Figure S6E).

Mutations outside of known RNA paths compromise exosome activity

The structure of Exo10^{6} bound to 24 nt polyA RNA revealed electron density for the 3′ RNA end in the Rrp6 active site followed by five nucleotides in addition to three partially modeled nucleotide positions that contact the S1/KH ring (23), suggesting that the remaining RNA was disordered. In the Exo12$^{44/6/47}$ structure bound to 18 nt AU-rich RNA (24), RNA was not observed in the Rrp6 active site, and bypassed it altogether. Although data were twinned and the resolution limiting (69.5% data completeness to 4.6 Å) for the Exo12$^{44/6/47}$ exosome structure, perhaps the RNA was not long enough to bridge contacts between Rrp6, the S1/KH cap and Rrp6 C-terminal tail. In contrast, and perhaps consistent with longer RNAs engaging in more extensive contact surfaces than observed in these structures, site-specific UV crosslinking with a 36-nucleotide RNA revealed contacts to all three S1/KH cap proteins and Rrp6, but not the PH-like ring subunits (23). To determine if the integrity of Exo9 surfaces between the lasso and Rrp6 catalytic domain contribute to activities (Figure 7A), mutations were selected between Rrp4, Mtr3, Rrp42, Csl4 and the HRDC/EAR domains of Rrp6 (23): two electrostatic substitutions for Csl4 R206D and Mtr3 K132E, and one substitution between Rrp6 and Csl4 in Rrp4 (W278A). Expression and purification of these mutant subunits in isolation and as reconstituted Exo9 complexes (Exo9^{3X}) were comparable to their wild-type counterparts (Supplementary Figure S7A).

Degradation of AU-rich and polyA RNAs is inhibited using Exo10$^{6\text{-}3X}$, but defects vary depending on the RNA substrate as Exo10$^{6\text{-}3X}$ is not active on polyA RNA, but displays some activity with AU-rich RNA (Figure 7B). Exo10^{6} was also reconstituted with two of the three substitutions: Mtr3 K132E and Rrp4 W278A (Exo10$^{6\text{-}2X}$). Exo10$^{6\text{-}2X}$ is more active than the triple mutant on AU-rich RNA; however, decay of polyA RNA remains deficient (Supplementary Figure S7B). To determine if defects observed for these mutations were dependent on the Rrp6 lasso, Exo10$^{6\text{Lassoless}}$ was reconstituted using Exo9 wild-type and Exo9^{3X}. Although mutations in the Exo9 cores diminished activities slightly for Exo10$^{6\text{Lassoless}}$ compared to wild-type Exo9 (Figure 7C), defects observed for mutations in the Rrp4/Mtr3/Csl4 interface appear more pronounced when the Rrp6 lasso is present (Figure 7B).

We next determined if these Exo9 mutations altered Rrp44 activities by reconstituting Rrp44 with Exo9^{3X}. Decay of AU-rich RNA by Exo10$^{44\text{-}3X}$ is slightly attenuated in comparison to wild-type Exo10^{44} (Figure 7B), perhaps consistent with the RNA path observed in the Exo11$^{44/6EAR}$ crystal structure (22) as RNA passes through the Exo9 central channel at a site distal from these mutations. However, in the presence of Rrp6^{exo-}, Exo11$^{44WT/6exo-}$ activities are markedly inhibited by the triple Exo9 point mutations, especially evident for the polyA RNA substrate (Figure 7B). Based on current structural models and biochemical data presented here, it is possible that the RNA path observed in Exo11$^{44/6EAR}$ (22) reflects one utilized in the cytoplasmic exosome (Exo10^{44}), while in the nuclear exosome (Exo11$^{44/6}$), the Rrp6 catalytic module and C-terminal lasso contribute to alternative surfaces that become important for guiding RNA through the Exo9 central channel (23,24), thereby providing alternative paths to accommodate RNA entry to the Rrp6 or Rrp44 active sites.

DISCUSSION

Studies presented here highlight a role for a previously unappreciated functional domain of Rrp6, its C-terminal region, or lasso, in binding RNA and stimulating RNA degradation by Rrp6 and Rrp44. Deletion of this highly basic 100 amino acid stretch diminishes Rrp6 activity, in and out of the exosome. The lasso also stimulates endo- and exoribonuclease activities of Rrp44, activities that remain dependent on the integrity of the central channel. Biochemical results suggest that the Rrp6 lasso and catalytic domain are required for Rrp6-mediated stimulation of Rrp44 activities, particularly on polyA RNA, as neither are sufficient to fully activate Rrp44 exoribonuclease activity on their own. Furthermore, yeast strains harboring lasso deletions exhibited growth defects in rich media, with altered processing and decay activities as assessed by analysis of some known exosome substrates, and synthetic growth defects when combined with mutations that compromise other exosome activities.

The highly basic Rrp6 lasso has no counterpart in prokaryotic RNase D family members (45), and appears to be a unique eukaryotic exosome-specific domain with biophysical (Supplementary Table S1) properties that appear conserved among eukaryotes (Figure 5B), despite lacking apparent sequence conservation (Supplementary Figure S2). In addition to being highly basic, however, sequences

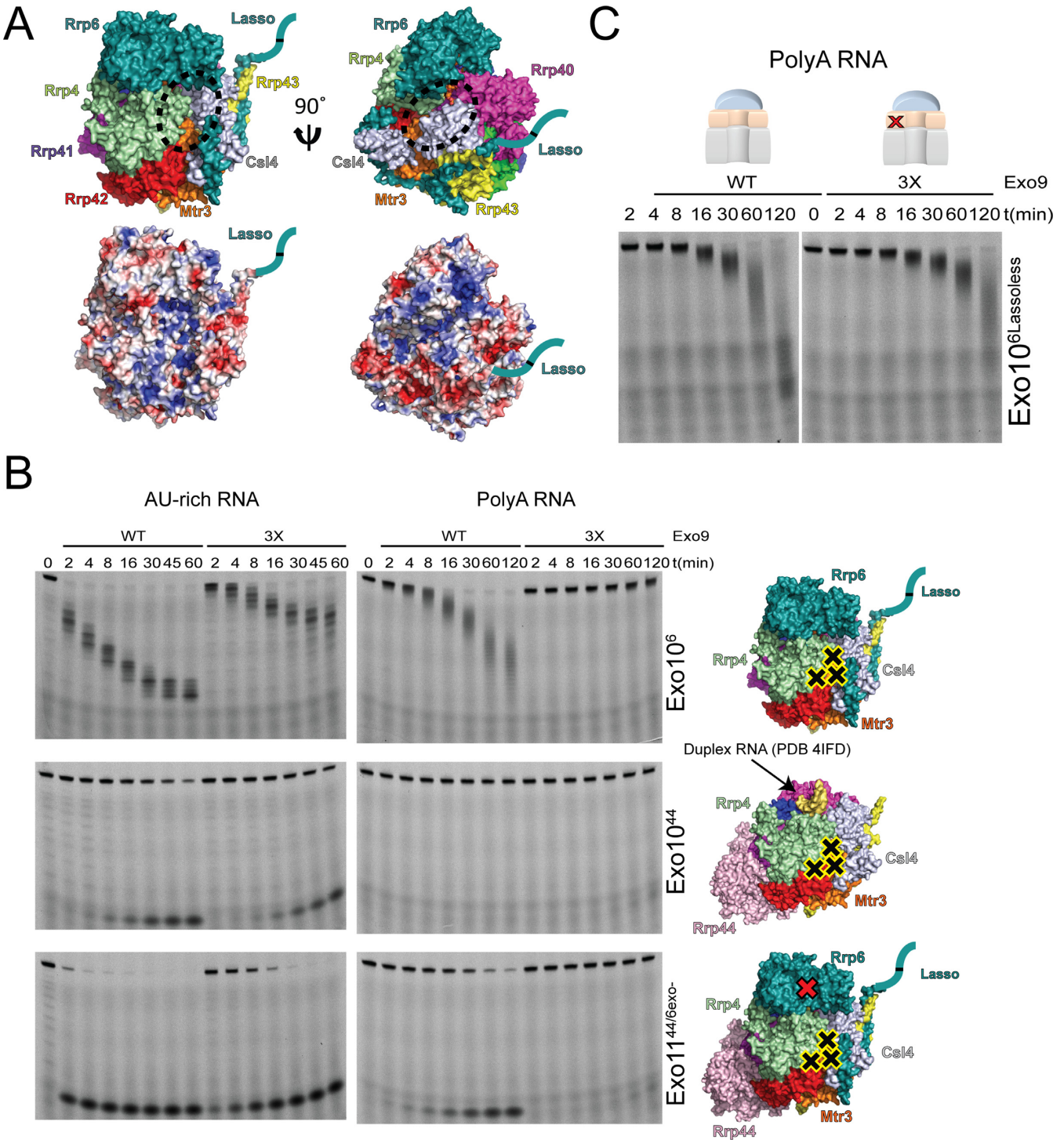

Figure 7. Mutations in Exo9 between the Rrp6 CAT and lasso are important for RNA decay in Exo10^{6} and Exo11$^{44/6}$. (**A**) The structure of Exo10^{6} bound to polyA RNA (PDB 4OO1), and presumed location of the Rrp6 lasso, suggested alternative surfaces formed by Rrp4, Mtr3, Rrp42 and Csl4 that were selected for mutational analysis (dashed circle). Structural models and electrostatics generated using PyMol and APBS (60), respectively. (**B**) Exo10^{6}, Exo10^{44} and Exo11$^{44WT/6exo-}$ activities on 5′ fluorescein 49 nt AU-rich (left) and polyA RNAs (right) comparing wild-type and Exo9 with three point mutations (Rrp4 W278A/Mtr3 K132E/Csl4 R206D). Mutations indicated as black crosses. Model of Exo10^{44} from PDB 4IFD, with the Rrp6 CTD removed, and an arrow pointing to the 5′ end of the bound duplex RNA that traverses the Exo9 central channel. Exo11$^{44/6}$ model generated from PDB codes 4OO1 and 4IFD. (**C**) Exo9^{3X} mutations exhibit diminished effects on Exo10^{6Lassoless} mediated decay of polyA RNA, suggesting that defects observed for Exo9^{3X} mutations are dependent on the Rrp6 lasso.

of the apparent eukaryotic Rrp6 lassoes also share putative nuclear localization sequences, motifs that have been shown here (Supplementary Figure S6A) and elsewhere (46,47) to double as nucleic acid interaction motifs. Furthermore, discrete sequences within the Rrp6 lasso in yeast and metazoans may bear resemblance to other RNA binding motifs known to be in disordered regions, including lysine-rich motifs (48), and eAT-hooks (49).

Given its ability to stimulate decay of longer RNAs, the Rrp6 lasso might provide additional RNA binding surfaces that assist in maintaining interactions with RNA during repeated encounters with the exosome and its catalytic activities. The importance of small, intrinsically disordered domains in large multi-subunit complexes and RNA binding proteins is gaining greater appreciation (50–56). While examples exist that can accelerate nucleic acid renaturation (57), the Rrp6 lasso has the opposite effect by stimulating RNA decay. Future work will be required to understand how it exerts this effect, perhaps most notably on structured RNA substrates of the nuclear RNA exosome.

SUPPLEMENTARY DATA

Supplementary Data are available at NAR Online.

ACKNOWLEDGEMENTS

The *rrp6Δ* strain in the W303 background was a gift from Michael Rosbash. The *rrp44Δrrp6Δ* strain in the S288C background was a gift from Jaeil Han and Ambro van Hoof. We thank Mom Das for the 5′-fluorescein labeled hypomodified initiator $tRNA_{iMet}$. E.V.W. initiated the project. E.V.W. and C.D.L designed experiments that E.V.W. performed. E.V.W. and C.D.L. wrote the manuscript. The content is solely the responsibility of the authors and does not represent the official views of the National Institutes of Health. C.D.L. is an investigator of the Howard Hughes Medical Institute.

FUNDING

National Institute of General Medical Sciences of the National Institutes of Health [F31GM097910 to E.V.W., R01GM079196 to C.D.L., R35GM118080 to C.D.L., P30 CA008748 to NIH NCI-Cancer Center Support Grant]. Funding for open access charge: HHMI/Institutional/NIH.
Conflict of interest statement. None declared.

REFERENCES

1. Houseley,J., LaCava,J. and Tollervey,D. (2006) RNA-quality control by the exosome. *Nat. Rev. Mol. Cell Biol.*, **7**, 529–539.
2. Kilchert,C., Wittmann,S. and Vasiljeva,L. (2016) The regulation and functions of the nuclear exosome complex. *Nat. Rev. Mol. Cell Biol.*, **17**, 227–239.
3. Anderson,J.S. and Parker,R.P. (1998) The 3′ to 5′ degradation of yeast mRNAs is a general mechanism for mRNA turnover that requires the SKI2 DEVH box protein and 3′ to 5′ exonucleases of the exosome complex. *EMBO J.*, **17**, 1497–506.
4. Allmang,C., Kufel,J., Chanfreau,G., Mitchell,P., Petfalski,E. and Tollervey,D. (1999) Functions of the exosome in rRNA, snoRNA and snRNA synthesis. *EMBO J.*, **18**, 5399–5410.
5. Allmang,C., Mitchell,P., Petfalski,E. and Tollervey,D. (2000) Degradation of ribosomal RNA precursors by the exosome. *Nucleic Acids Res.*, **28**,1684–1691.
6. van Hoof,A., Lennertz,P. and Parker,R. (2000) Yeast exosome mutants accumulate 3′-extended polyadenylated forms of U4 small nuclear RNA and small nucleolar RNAs. *Mol. Cell. Biol.*, **20**, 441–452.
7. Wyers,F., Rougemaille,M., Badis,G., Rousselle,J.C., Dufour,M.E., Boulay,J., Régnault,B., Devaux,F., Namane,A., Séraphin,B. *et al.* (2005) Cryptic pol II transcripts are degraded by a nuclear quality control pathway involving a new poly(A)polymerase. *Cell*, **121**, 725–737.
8. Davis,C.A. and Ares,M. Jr (2006) Accumulation of unstable promoter-associated transcripts upon loss of the nuclear exosome subunit Rrp6p in Saccharomyces cerevisiae. *Proc. Natl. Acad. Sci. U.S.A.*, **103**, 3262–3267.
9. Neil,H., Malabat,C., d'Aubenton-Carafa,Y., Xu,Z., Steinmetz,L.M. and Jacquier,A. (2009) Widespread bidirectional promoters are the major source of cryptic transcripts in yeast. *Nature*, **457**,1038–1042.
10. Xu,Z., Wei,W., Gagneur,J., Perocchi,F., Clauder-Münster,S., Camblong,J., Guffanti,E., Stutz,F., Huber,W. and Steinmetz,L.M. (2009) Bidirectional promoters generate pervasive transcription in yeast. *Nature*, **457**, 1033–1037.
11. Bühler,M., Haas,W., Gygi,S.P. and Moazed,D. (2007) RNAi-dependent and -independent RNA turnover mechanisms contribute to heterochromatic gene silencing. *Cell*, **129**, 707–721.
12. Januszyk,K. and Lima,C.D. (2014) The eukaryotic exosome. *Curr. Opin. Struct. Biol.*, **24**, 132–140.
13. Wasmuth,E.V. and Lima,C.D. (2012) Exo- and endoribonucleolytic activities of yeast cytoplasmic and nuclear RNA exosomes are dependent on the noncatalytic core and central channel. *Mol. Cell*, **48**, 133–144.
14. Lorentzen,E., Basquin,J., Tomecki,R., Dziembowski,A. and Conti,E. (2008) Structure of the active subunit of the yeast exosome core, Rrp44: diverse modes of substrate recruitment in the RNase II nuclease family. *Mol. Cell*, **29**, 717–728.
15. Lebreton,A., Tomecki,R., Dziembowski,A. and Séraphin,B. (2008) Endonucleolytic RNA cleavage by a eukaryotic exosome. *Nature*, **456**, 993–996.
16. Schaeffer,D., Tsanova,B., Barbas,A., Reis,F.P., Dastidar,E.G., Sanchez-Rotunno,M., Arraiano,C.M. and van Hoof,A. (2009) The exosome contains domains with specific endoribonuclease, exoribonuclease and cytoplasmic mRNA decay activities. *Nat. Struct. Mol. Biol.*, **16**, 56–62.
17. Schneider,C., Leung,E., Brown,J. and Tollervey,D. (2009) The N-terminal PIN domain of the exosome subunit Rrp44 harbors endonuclease activity and tethers Rrp44 to the yeast core exosome. *Nucleic Acids Res.*, **37**, 1127–1140.
18. Midtgaard,S.F., Assenholt,J., Jonstrup,A.T., Van,L.B., Jensen,T.H. and Brodersen,D.E. (2006) Structure of the nuclear exosome component Rrp6p reveals an interplay between the active site and the HRDC domain. *Proc. Natl. Acad. Sci. U.S.A.*, **103**, 11898–11903.
19. Stead,J.A., Costello,J.L., Livingstone,M.J. and Mitchell,P. (2007) The PMC2NT domain of the catalytic exosome subunit Rrp6p provides the interface for binding with its cofactor Rrp47p, a nucleic acid-binding protein. *Nucleic Acids Res.*, **35**, 5556–5567.
20. Feigenbutz,M., Garland,W., Turner,M. and Mitchell,P. (2013) The exosome cofactor Rrp47 is critical for the stability and normal expression of its associated exoribonuclease Rrp6 in Saccharomyces cerevisiae. *PLoS One*, **8**, e80752.
21. Schuch,B., Feigenbutz,M., Makino,D.L., Falk,S., Basquin,C., Mitchell,P. and Conti,E. (2014) The exosome-binding factors Rrp6 and Rrp47 form a composite surface for recruiting the Mtr4 helicase. *EMBO J.*, **33**, 2829–2846.
22. Makino,D.L., Baumgärtner,M. and Conti,E. (2013) Crystal structure of an RNA-bound 11-subunit eukaryotic exosome complex. *Nature*, **495**, 70–75.
23. Wasmuth,E.V., Januszyk,K.J. and Lima,C.D. (2014) Structure of an Rrp6-RNA exosome complex bound to poly(A) RNA. *Nature*, **511**, 435–439.
24. Makino,D.L., Schuch,B., Stegmann,E., Baumgärtner,M., Basquin,C. and Conti,E. (2015) RNA degradation paths in a 12-subunit nuclear exosome complex. *Nature*, **524**, 54–58.

25. Phillips,S. and Butler,J.S. (2003) Contribution of domain structure to the RNA 3′ end processing and degradation functions of the nuclear exosome subunit Rrp6p. *RNA*, **9**, 1098–1107.
26. Liu,J.J., Bratkowski,M.A., Liu,X., Niu,C.Y., Ke,A. and Wang,H.W. (2013) Visualization of distinct substrate-recruitment pathways in the yeast exosome by EM. *Nat. Struct. Mol. Biol.*, **21**, 95–102.
27. Drążkowsak,K., Tomecki,R., Stodus,K., Kowalska,K., Czarnocki-Cieciura,M. and Dziembowski,A. (2013) The RNA exosome complex central channel controls both exonuclease and endonuclease Dis3 activities in vivo and in vitro. *Nucleic Acids Res.*, **41**, 3845–3858.
28. Greimann,J.C. and Lima,C.D. (2008) Reconstitution of RNA exosomes from human and Saccharomyces cerevisiae cloning, expression, purification, and activity assays. *Methods Enzymol.*, **448**, 185–210.
29. Liu,Q., Greimann,J.C. and Lima,C.D. (2006) Reconstitution, activities, and structure of the eukaryotic RNA exosome. *Cell*, **127**, 1223–1237.
30. Senger,B., Despons,L., Walter,P. and Fasiolo,F. (1992) The anticodon triplet is not sufficient to confer methionine acceptance to a transfer RNA. *Proc. Natl. Acad. Sci. U.S.A.*, **89**, 10768–10771.
31. Wang,X., Jia,H., Jankowsky,E. and Anderson,J.T. (2008) Degradation of hypomodified tRNA (iMet) in vivo involves RNA-dependent ATPase activity of the DExH helicase Mtr4p. *RNA*, **14**, 107–116.
32. Zearfoss,N. R. and Ryder,S. P. (2012) End-labeling oligonucleotides with chemical tags after synthesis. *Methods Mol. Biol.*, **941**, 181–193.
33. Abruzzi,K., Denome,S., Olsen,J.R., Assenholt,J., Haaning,L.L, Jensen,T.H. and Rosbash,M. (2007) A novel plasmid-based microarray screen identifies suppressors of rrp6Delta in Saccharomyces cerevisiae. *Mol. Cell. Biol.*, **27**, 1044–1055.
34. LaCava,J., Houseley,J., Saveanu,C., Petfalski,E., Thompson,E., Jacquier,A. and Tollervey,D. (2005) RNA degradation by the exosome is promoted by a nuclear polyadenylation complex. *Cell*, **121**, 713–724.
35. Kadaba,S., Kreuger,A., Trice,T., Krecic,A.M., Hinnebusch,A.G. and Anderson,J. (2004) Nuclear surveillance and degradation of hypomodified initiator $tRNA^{Met}$ in *S. cerevisiae*. *Genes Dev.*, **18**, 1224–1240.
36. Basavappa,R. and Sigler,B.P. (1991) The 3 Å crystal structure of yeast initiator tRNA: functional implications in initiator/elongator discrimination. *EMBO J.*, **10**, 3105–3111.
37. Bonneau,F., Basquin,J., Ebert,J., Lorentzen,E. and Conti,E. (2009) The yeast exosome functions as a macromolecular cage to channel RNA substrates for degradation. *Cell*, **139**, 547–559.
38. Callahan,K.P. and Butler,J.S. (2008) Evidence for core exosome independent function of the nuclear exoribonuclease Rrp6p. *Nucleic Acids Res.*, **36**, 6645–6655.
39. Klauer,A.A. and van Hoof,A. (2013) Genetic interactions suggest multiple distinct roles of the arch and core helicase domains of Mtr4 in Rrp6 and exosome function. *Nucleic Acids Res.*, **41**, 533–541.
40. Castelnuovo,M., Rahman,S., Guffanti,E., Infantino,V., Stutz,F. and Zenklusen,D. (2013) Bimodal expression of PHO84 is modulated by early termination of antisense transcription. *Nat. Struct. Mol. Biol.*, **20**, 851–858.
41. Ming-Hsiu,H., Mittmann,M., Dong,H., Wodicka,L. and Lockhart,D.J. (1997) Genome-wide expression monitoring in Saccharomyces cerevisiae. *Nat. Biotech.*, **15**, 1359–1367.
42. Feigenbutz,M., Jones,R., Besong,T.M., Harding,S.E. and Mitchell,P. (2013) Assembly of the yeast exoribonuclease Rrp6 with its associated cofactor Rrp47 occurs in the nucleus and is critical for the controlled expression of Rrp47. *J Biol Chem*, **288**, 15959–15970.
43. Assenholt,J., Mouaikel,J., Andersen,K.R., Brodersen,D.E., Libri,D. and Jensen,T.H. (2008) Exonucleolysis is required for nuclear mRNA quality control in yeast THO mutants. *RNA*, **14**, 2305–2313.
44. Dziembowski,A., Lorentzen,E., Conti,E. and Seraphin,B. (2007) A single subunit, Dis3, is essentially responsible for yeast exosome core activity. *Nat. Struct. Mol. Biol.*, **14**, 15–22.
45. Zuo,Y., Wang,Y. and Malhotra,A. (2005) Crystal structure of Escherichia coli RNase D, an exoribonuclease involved in structured RNA processing. *Structure*, **13**, 973–984.
46. LaCasse,E.C. and Lefebvre,Y.A. (1995) Nuclear localization signals overlap DNA- or RNA-binding domains in nucleic acid-binding proteins. *Nucleic Acids Res.*, **23**, 1647–1656.
47. Yao,K., Wu,Y., Chen,Q., Zhang,Z., Chen,X. and Zhang,Y. (2016) The Arginine/Lysine-rich element within the DNA-binding domain is essential for nuclear localization and function of the intracellular pathogen resistance 1. *PLoS One*, **11**, e0162832.
48. Castello,A., Fischer,B., Frese,C.K., Horos,R., Alleaume,A.M., Foehr,S., Curk,T., Krijgsveld,J. and Hentze,M.W. (2016) Comprehensive identification of RNA-Binding domains in human cells. *Mol . Cell*, **63**, 696–710.
49. Filarsky,M., Zillner,K., Araya,I., Villar-Garea,A., Merkl,R., Langst,G. and Nemeth,A. (2015) The extended AT-hook is a novel RNA binding motif. *RNA Biol.*, **12**, 864–876.
50. Melnikov,S., Ben-Shem,A., Yusupova,G. and Yusupov,M. (2015) Insights into the origin of the nuclear localization signals in conserved ribosomal proteins. *Nat. Commun.*, **6**, 7382.
51. Tomko,R.J. Jr and Hochstrasser,M. (2014) The intrinsically disordered Sem1 protein functions as a molecular tether during proteasome lid biogenesis. *Mol. Cell*, **53**, 433–443.
52. Kucera,N.J., Hodsdon,M.E. and Wolin,S.L. (2011) An intrinsically disordered C terminus allows the La protein to assist the biogenesis of diverse noncoding RNA precursors. *Proc. Natl. Acad. Sci. U.S.A.*, **108**, 1308–1313.
53. Varadi,M., Zsolyomi,F., Guharoy,M. and Tompa,P. (2015) Functional advantages of conserved intrinsic disorder in RNA-Binding proteins. *PLoS One*, **10**, e0139731.
54. Calabretta,S. and Richard,S. (2015) Emerging roles of disordered sequences in RNA-Binding proteins. *Trends Biochem Sci.*, **40**, 662–72.
55. Castello,A., Fischer,B., Eichelbaum,K., Horos,R., Beckmann,B.M., Strein,C., Davey,N.E., Humphreys,D.T., Preiss,T., Steinmetz,L.M. *et al.* (2012) Insights into RNA biology from an atlas of mammalian mRNA-binding proteins. *Cell*, **149**, 1393–1406.
56. Jonas,S. and Izaurralde,E. (2013) The role of disordered protein regions in the assembly of decapping complexes and RNP granules. *Genes Dev.*, **27**, 2628–2641.
57. Tompa,P. and Csermely,P. (2004) The role of structural disorder in the function of RNA and protein chaperones. *FASEB J.*, **18**,1169–1175.
58. Larkin,M.A. *et al.* ClustalW and ClustalX Version 2. (2007) *Bioinformatics*, **23**, 2947–2948.
59. Gasteiger,E., Hoogland,C., Gattiker,A., Duvaud,S., Wilkins,M.R., Appel,R.D. and Bairoch,A. (2005) Protein identification and analysis tools on the ExPASy Server. In: Walker,JM (ed). *The Proteomics Protocols Handbook*. Humana Press, Totowa, pp. 571–607.
60. Baker,N.A., Sept,D., Joseph,S., Holst,M.J. and McCammon,J.A. (2001) Electrostatics of nanosystems: application to microtubules and the ribosome. *Proc. Natl. Acad. Sci. U.S.A.*, **98**, 10037–10041.